

Analysis of AlN/AlGaIn/GaN metal-insulator-semiconductor structure by using capacitance-frequency-temperature mapping

Hong-An Shih, Masahiro Kudo, and Toshi-kazu Suzuki^{a)}

Center for Nano Materials and Technology, Japan Advanced Institute of Science and Technology (JAIST),
1-1 Asahidai, Nomi, Ishikawa 923-1292, Japan

(Received 7 June 2012; accepted 5 July 2012; published online 24 July 2012)

AlN/AlGaIn/GaN metal-insulator-semiconductor (MIS) structure is analyzed by using capacitance-frequency-temperature (C - f - T) mapping. Applying sputtering-deposited AlN, we attained AlN/AlGaIn/GaN MIS heterostructure field-effect transistors with much suppressed gate leakage currents, but exhibiting frequency dispersion in C - V characteristics owing to high-density AlN/AlGaIn interface states. In order to investigate the interface states deteriorating the device performance, we measured temperature-dependent frequency dispersion in the C - V characteristics. As a result, we obtained C - f - T mapping, whose analysis gives the activation energies of electron trapping, namely the interface state energy levels, for a wide range of the gate biases. This analysis method is auxiliary to the conventional conductance method, serving as a valuable tool for characterization of wide-bandgap devices with deep interface states. From the analysis, we can directly evaluate the gate-control efficiency of the devices. © 2012 American Institute of Physics.
[<http://dx.doi.org/10.1063/1.4737876>]

AlGaIn/GaN heterojunction field-effect transistors (HFETs)¹ have been extensively developed as promising devices for high-frequency and high-power applications. However, gate leakage current is a limiting factor for practical usage of these devices. In order to solve this problem, AlGaIn/GaN metal-insulator-semiconductor (MIS) HFETs, enabling effective reduction of the gate leakage currents, have been developed and studied. In particular, high-dielectric-constant (high- k) oxide materials, such as Al₂O₃ (Ref. 2) or HfO₂ (Refs. 3 and 4), have been investigated as a gate insulator of the MIS-HFETs. On the other hand, AlN is an important high- k non-oxide insulator possessing possible suitability for III-V device processing.^{5,6} In addition to AlN-passivated AlGaIn/GaN HFETs exhibiting good heat release properties^{7–12} due to the high thermal conductivity of AlN (~ 10 times higher than that of Al₂O₃),¹³ AlN/AlGaIn/GaN MIS-HFETs, where the AlN gate insulator was sputtering-deposited, have been investigated,^{7,14,15} owing to a possible high breakdown field $\gtrsim 10$ MV/cm (Refs. 16 and 17) and a high dielectric constant ~ 10 (Ref. 18) comparable to those of Al₂O₃. In particular, we showed significant suppression of gate leakage current, although frequency dispersion in the C - V characteristics for forward gate biases was observed.¹⁵ This dispersion is attributed to high-density AlN/AlGaIn interface mid-gap states leading to a gate-control impediment, which severely depresses the device performances. Such mid-gap states in GaN-based devices have been investigated by Terman method,^{19–21} conductance method,^{14,15,22–27} and deep level transient spectroscopy (DLTS).^{28–31} In the previous work, we employed the conductance method for analysis of capacitance-voltage-frequency (C - V - f) characteristics to investigate the AlN/AlGaIn interface state density and electron trapping time constant at room temperature.¹⁵ In this work, we propose an analysis

method using capacitance-frequency-temperature (C - f - T) mapping obtained from the temperature-dependent C - V - f characteristics. This method gives the activation energies of electron trapping, namely the interface state energy levels, for a much extended range of the gate biases, serving as an auxiliary tool to the conventional conductance method.

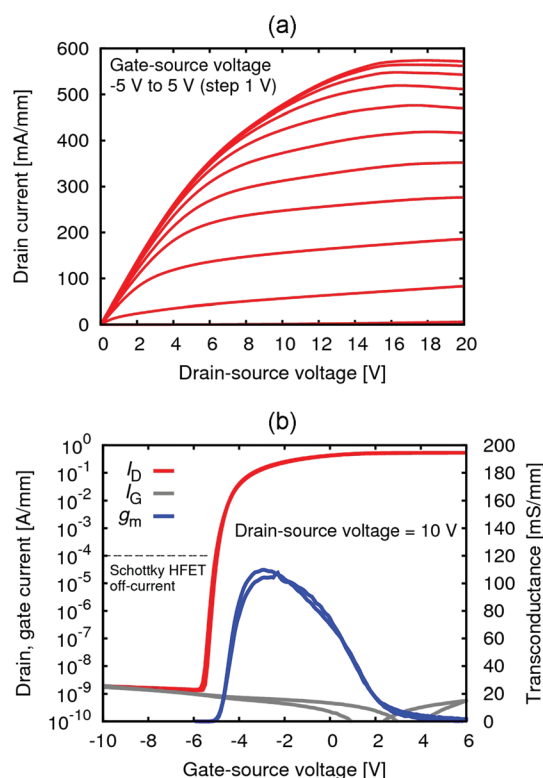


FIG. 1. Characteristics of the AlN/AlGaIn/GaN MIS-HFET. (a) Output characteristics. (b) Transfer characteristics, where drain current I_D , gate current I_G , and transconductance g_m were obtained under the gate voltage sweep of $-10 \text{ V} \rightarrow +6 \text{ V} \rightarrow -10 \text{ V}$.

^{a)} Author to whom correspondence should be addressed. Electronic mail: tosikazu@jaist.ac.jp.

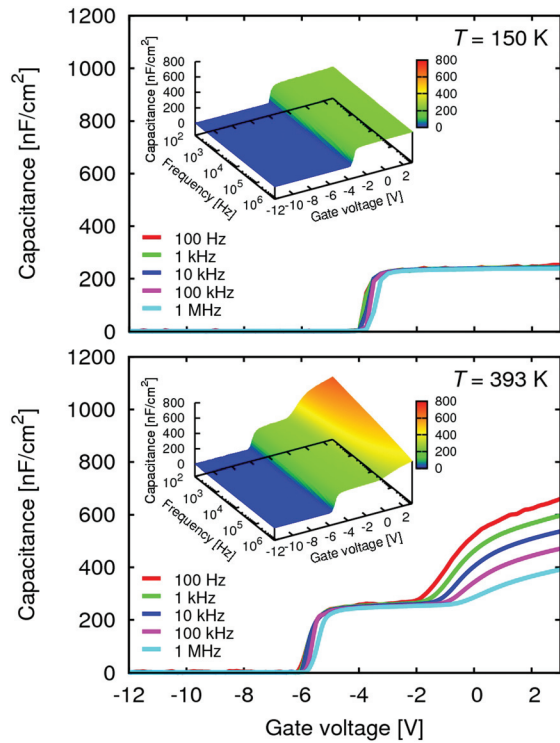


FIG. 2. C - V - f characteristics of the AlN/AlGaIn/GaN MIS structure at 150 K (above) and 393 K (below).

Moreover, from the interface state energy levels corresponding to a wide range of the gate biases, we can directly evaluate the gate-control efficiency of the devices.

We fabricated AlN/AlGaIn/GaN MIS-HFETs and MIS structures simultaneously using an $\text{Al}_{0.29}\text{Ga}_{0.71}\text{N}$ (25 nm)/GaIn (3000 nm) heterostructure obtained by metal-organic vapor phase epitaxy on sapphire(0001). Hall measurements of the heterostructure show an as-grown electron mobility of $1200 \text{ cm}^2/\text{V}\cdot\text{s}$ and a sheet electron concentration of $1.3 \times 10^{13} \text{ cm}^{-2}$. On the heterostructure, Ti/Al/Ti/Au Ohmic electrodes were formed and device isolation was achieved by B^+ implantation. On the AlGaIn surface cleaned by organic solvents, deionized water, and oxygen plasma ashing to remove surface organic contaminants, followed by oxide removal using Semicoclean (ammonium-based etchant), an AlN gate insulator of $\sim 19 \text{ nm}$ thickness was deposited by RF magnetron sputtering at room temperature with an AlN target in Ar- N_2 ambient. The formation of Ni/Au gate electrodes completed the device fabrication. The MIS-HFETs have the gate length of 250 nm, the source-gate spacing of 2 μm , the gate-drain spacing of 3 μm , and the gate width of 50 μm , while the MIS structures have the 100 $\mu\text{m} \times 100 \mu\text{m}$ gate electrode surrounded by the Ohmic electrode.

In Figs. 1(a) and 1(b), we show output and transfer characteristics of the fabricated MIS-HFET, respectively. Owing to good insulating properties of the AlN, gate leakage currents are significantly small, 10^{-9} A/mm range or less, for both reverse and forward gate biases. The small gate leakage currents lead to small drain off-currents shown in Fig. 1(b). However, we observe a rapid decrease in the transconductance towards forward gate biases, suggesting high-density AlN/AlGaIn interface states.

In order to investigate the AlN/AlGaIn interface states, we measured the C - V - f characteristics between the 100 $\mu\text{m} \times 100 \mu\text{m}$ gate electrode and the grounded Ohmic electrode surrounding the gate of the MIS structure at temperatures from 150 K to 393 K. Figure 2 shows the C - V - f characteristics at 150 K and 393 K. At 393 K, we observe a significant frequency dispersion for forward gate biases, which is attributed to electron trapping at interface states, while the frequency dispersion disappears at 150 K because of much longer electron trapping time constants. To characterize the interface states quantitatively, we carried out an analysis using the conductance method³² based on the equivalent circuit of the MIS structures depicted in the inset of Fig. 3 (top), with the insulator capacitance C_0 , the semiconductor capacitance C_s , the interface state capacitance C_i , and the interface state conductance G_i . Using the interface state density D_i and the electron trapping time constant τ , we obtain³³

$$C_i = \frac{q^2 D_i \arctan(\omega\tau)}{\omega\tau} \quad (1)$$

and

$$\frac{G_i}{\omega} = \frac{q^2 D_i \ln(1 + \omega^2\tau^2)}{2\omega\tau}, \quad (2)$$

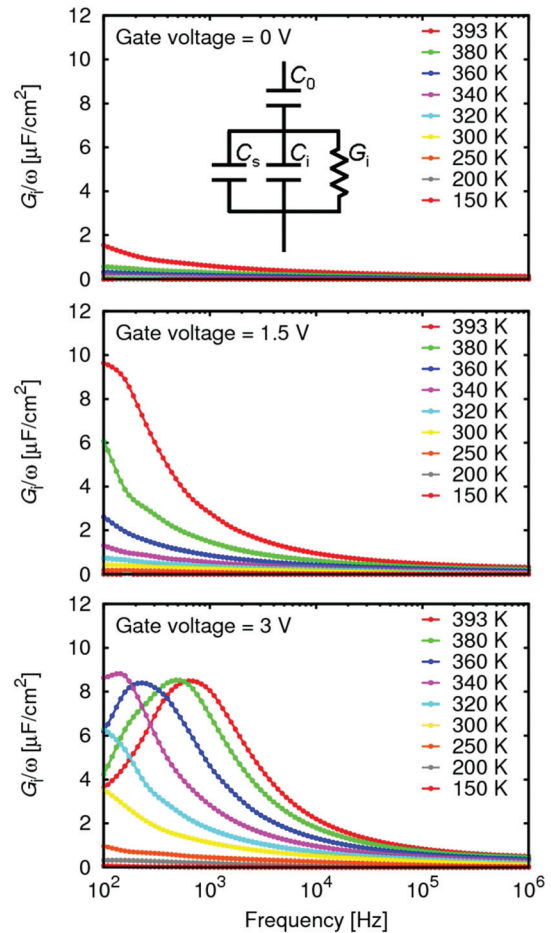


FIG. 3. Frequency dependence of G_i/ω for temperatures from 393 K to 150 K at gate voltages of 0 V (top), 1.5 V (middle), and 3 V (bottom). Top inset: the equivalent circuit of the MIS structures.

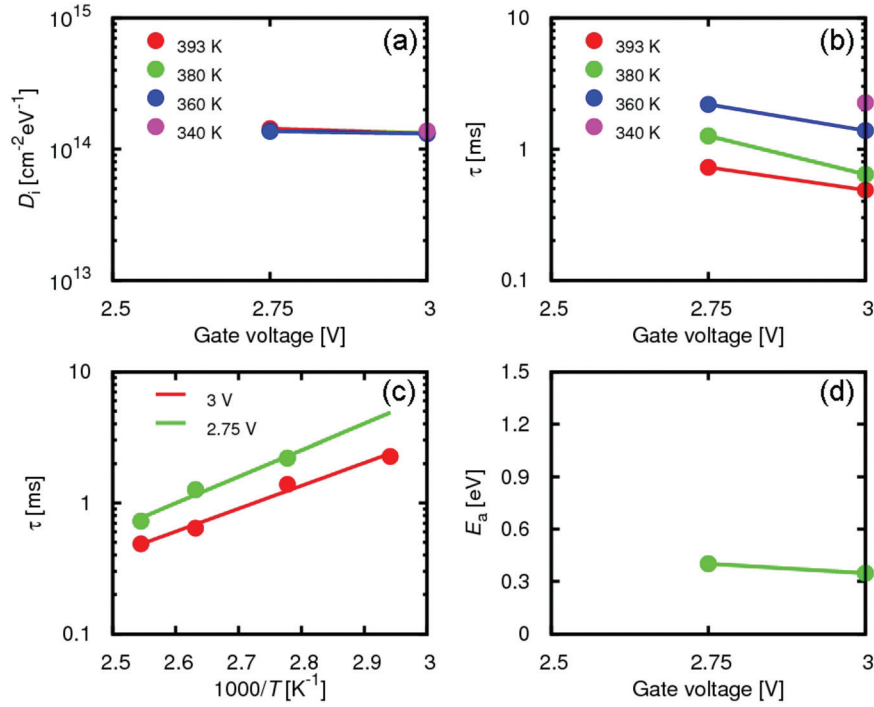


FIG. 4. (a) Interface state density D_i and (b) electron trapping time constant τ , obtained from the peak values and positions of the frequency-dependent G_i/ω based on the conductance method. (c) The Arrhenius plot of the temperature-dependent τ . (d) The activation energy E_a as a function of gate voltage, obtained from the Arrhenius plot (c).

where q is the electron charge and $\omega = 2\pi f$ is the angular frequency; G_i/ω as a function of frequency exhibits a single-peaked behavior, with the peak frequency $\sim 1/\pi\tau$ and the

peak value $\sim 0.4q^2D_i$. Assuming the designed value of the insulator capacitance $C_0 = 610 \text{ nF/cm}^2$, we show frequency dependence of G_i/ω , for several temperatures and gate voltages of 0 V, 1.5 V, and 3 V, in Fig. 3. As the gate voltage decreases, the number of peaks decreases due to longer time constants for deeper interface state energy levels. Thus, only a narrow range of the gate biases gives peaks in the measured frequency and temperature range; most peaks are below

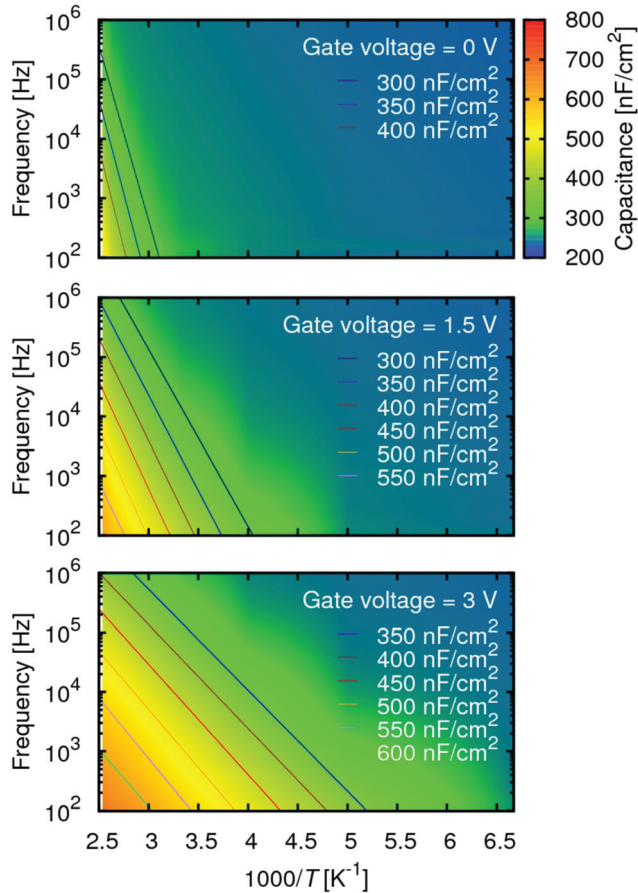


FIG. 5. C - f - T mappings with contours at gate voltages of 0 V (top), 1.5 V (middle), and 3 V (bottom).

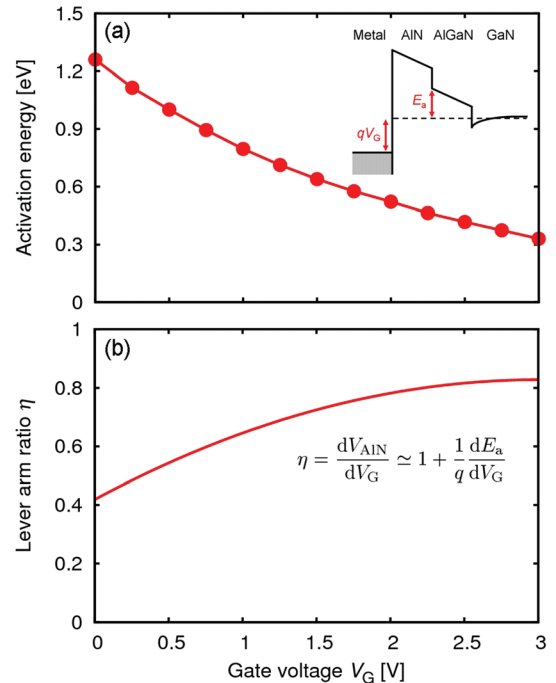


FIG. 6. (a) Gate voltage V_G dependence of the activation energy E_a extracted from the contours in C - f - T mappings. Inset: illustration of the bandbending and E_a . (b) Lever arm ratio $\eta = dV_{\text{AlIn}}/dV_G \simeq 1 + q^{-1}dE_a/dV_G$.

100 Hz due to significantly long time constants for the wide bandgap of AlGaIn/GaN systems. From the few peak positions and values, D_i and τ for temperatures of 340–393 K are obtained as shown in Figs. 4(a) and 4(b), respectively, where $D_i \sim 10^{14} \text{ cm}^{-2} \text{ eV}^{-1}$ and $\tau \sim \text{ms}$. From the Arrhenius plot of the temperature dependence of τ shown in Fig. 4(c), given by $\tau = \tau_0 \exp(E_a/k_B T) = \tau_0 \exp(\beta E_a)$, we extracted the activation energy E_a shown in Fig. 4(d) and estimated $\tau_0 \sim 10 \text{ ns}$. However, we have a problem that the conventional conductance method to investigate interface states is available only for a narrow range of gate biases, prohibiting the analysis of deeper interface states.

In order to solve the problem, we propose an analysis method using C - f - T mapping obtained from the temperature-dependent C - V - f characteristics. In Fig. 5, we show the C - f - T mappings at gate voltages of 0 V, 1.5 V, and 3 V, with contours. The contours exhibit a straight line behavior, which can be explained by the equivalent circuit of the MIS structures with a total admittance

$$Y = \frac{1}{Z} = \left(\frac{1}{jC_0\omega} + \frac{1}{G_i + jC_s\omega + jC_i\omega} \right)^{-1}. \quad (3)$$

Since C_i given by Eq. (1) and G_i/ω by Eq. (2) are functions of only $\omega\tau$, the measured capacitance $C = \text{Im}Y/\omega$ is a function of only $\omega\tau$. Therefore, a contour in C - f - T mapping, i.e., $C = \text{constant}$ leading to $\omega\tau = 2\pi f\tau = \text{constant}$, exhibits a straight line behavior as expressed by $f \propto 1/\tau \propto \exp(-\beta E_a)$, from which the activation energy E_a corresponding to the interface state energy level can be extracted. Figure 6(a) shows the gate voltage V_G dependence of E_a extracted from the contours in the C - f - T mappings, with the inset illustrating the bandbending and E_a . In addition to the fact that the obtained values of E_a for the gate voltage $\geq 2.75 \text{ V}$ are in good agreement with those obtained by the conductance method, we find that E_a can be obtained for a much extended range of the gate biases. This is due to slow $\omega\tau$ dependence of Eqs. (1) and (2); even though the frequency is far from the peak position $\sim 1/\pi\tau$, change in the C - f - T mapping is detectable. Furthermore, from the interface state energy levels corresponding to a wide range of the gate biases, the gate-control efficiency of the devices can be directly evaluated from the derivative dE_a/dV_G . As shown in the inset of Fig. 6(a), the gate voltage change ΔV_G is divided by the AlN gate insulator with ΔV_{AIN} and AlGaIn/GaN. Since $\Delta V_G \simeq \Delta V_{\text{AIN}} - \Delta E_a/q$, we obtain a “lever arm ratio” $\eta = dV_{\text{AIN}}/dV_G \simeq 1 + q^{-1}dE_a/dV_G$ as shown in Fig. 6(b). We find that small negative values of dE_a/dV_G give large values of η near the unity corresponding to poor gate-control efficiencies. This analysis method is important as an auxiliary tool to the conventional conductance method.

In summary, we analyzed the AlN/AlGaIn/GaN MIS-HFETs using C - f - T mapping for the investigation of AlN/AlGaIn interface states. The analysis method gives the activation energies of electron trapping, namely the interface

state energy levels, for a wide range of the gate biases. This method is auxiliary to the conventional conductance method, serving as a valuable tool for characterization of wide-bandgap devices with deep interface states. Furthermore, the method also enables a direct evaluation of the gate-control efficiency of the devices.

- ¹M. Khan, A. Bhattarai, J. Kuznia, and D. Olson, *Appl. Phys. Lett.* **63**, 1214 (1993).
- ²T. Hashizume, S. Ootomo, and H. Hasegawa, *Appl. Phys. Lett.* **83**, 2952 (2003).
- ³C. Liu, E. F. Chor, and L. S. Tan, *Appl. Phys. Lett.* **88**, 173504 (2006).
- ⁴A. Kawano, S. Kishimoto, Y. Ohno, K. Maezawa, T. Mizutani, H. Ueno, T. Ueda, and T. Tanaka, *Phys. Status Solidi C* **4**, 2700 (2007).
- ⁵K. Saito, T. Ono, M. Shimada, N. Shigekawa, and T. Enoki, *Jpn. J. Appl. Phys.* **44**, 334 (2005).
- ⁶M. Kudo, H.-A. Shih, M. Akabori, and T. Suzuki, *Jpn. J. Appl. Phys.* **51**, 02BF07 (2012).
- ⁷Y. Liu, J. A. Bardwell, S. P. McAlister, S. Rolfe, H. Tang, and J. B. Webb, *Phys. Status Solidi C* **0**, 69 (2002).
- ⁸J. Hwang, W. Schaff, B. Green, H. Cha, and L. Eastman, *Solid-State Electron.* **48**, 363 (2004).
- ⁹N. Tanaka, H. Takita, Y. Sumida, and T. Suzuki, *Phys. Status Solidi C* **5**, 2972 (2008).
- ¹⁰N. Tanaka, Y. Sumida, H. Kawai, and T. Suzuki, *Jpn. J. Appl. Phys.* **48**, 04C099 (2009).
- ¹¹N. Tsurumi, H. Ueno, T. Murata, H. Ishida, Y. Uemoto, T. Ueda, K. Inoue, and T. Tanaka, *IEEE Trans. Electron Devices* **57**, 980 (2010).
- ¹²S. Huang, Q. Jiang, S. Yang, C. Zhou, and K. Chen, *IEEE Electron Device Lett.* **33**, 516 (2012).
- ¹³G. Slack, R. Tanzilli, R. Pohl, and J. Vandersande, *J. Phys. Chem. Solids* **48**, 641 (1987).
- ¹⁴R. Stoklas, D. Gregušová, Š. Gaži, J. Novák, and P. Kordoš, *J. Vac. Sci. Technol. B* **29**, 01A809 (2011).
- ¹⁵H.-A. Shih, M. Kudo, M. Akabori, and T. Suzuki, *Jpn. J. Appl. Phys.* **51**, 02BF01 (2012).
- ¹⁶L. Lipkin and J. Palmour, *IEEE Trans. Electron Devices* **46**, 525 (1999).
- ¹⁷T. Adam, J. Kolodzey, C. Swann, M. Tsao, and J. Rabolt, *Appl. Surf. Sci.* **175–176**, 428 (2001).
- ¹⁸M.-A. Dubois and P. Mural, *Appl. Phys. Lett.* **74**, 3032 (1999).
- ¹⁹Y. Chiou, S. Chang, Y. Su, C. Wang, T. Lin, and B.-R. Huang, *IEEE Trans. Electron Devices* **50**, 1748 (2003).
- ²⁰M. Miczek, C. Mizue, T. Hashizume, and B. Adamowicz, *J. Appl. Phys.* **103**, 104510 (2008).
- ²¹C. Mizue, Y. Hori, M. Miczek, and T. Hashizume, *Jpn. J. Appl. Phys.* **50**, 021001 (2011).
- ²²E. J. Miller, X. Z. Dang, H. H. Wieder, P. M. Asbeck, E. T. Yu, G. J. Sullivan, and J. M. Redwing, *J. Appl. Phys.* **87**, 8070 (2000).
- ²³R. M. Chu, Y. G. Zhou, K. J. Chen, and K. M. Lau, *Phys. Status Solidi C* **0**, 2400 (2003).
- ²⁴L. Semra, A. Telia, and A. Soltani, *Surf. Interface Anal.* **42**, 799 (2010).
- ²⁵B. Gaffey, L. Guido, X. Wang, and T. Ma, *IEEE Trans. Electron Devices* **48**, 458 (2001).
- ²⁶R. Stoklas, D. Gregušová, J. Novák, A. Vescan, and P. Kordos, *Appl. Phys. Lett.* **93**, 124103 (2008).
- ²⁷J. J. Freedman, T. Kubo, and T. Egawa, *Appl. Phys. Lett.* **99**, 033504 (2011).
- ²⁸T. Mizutani, H. Makihara, M. Akita, Y. Ohno, S. Kishimoto, and K. Maezawa, *Jpn. J. Appl. Phys.* **42**, 424 (2003).
- ²⁹M. Faqir, G. Verzellesi, F. Fantini, F. Danesin, F. Rampazzo, G. Meneghesso, E. Zanoni, A. Cavallini, A. Castaldini, N. Labat, A. Touboul, and C. Dua, *Microelectron. Reliab.* **47**, 1639 (2007).
- ³⁰Y. Nakano and T. Jimbo, *Appl. Phys. Lett.* **80**, 4756 (2002).
- ³¹T. Okino, M. Ochiai, Y. Ohno, S. Kishimoto, K. Maezawa, and T. Mizutani, *IEEE Electron Device Lett.* **25**, 523 (2004).
- ³²E. H. Nicollian and J. R. Brews, *MOS (Metal Oxide Semiconductor) Physics and Technology* (Wiley-Interscience, Hoboken, New Jersey, 1982).
- ³³K. Lehovec, *Appl. Phys. Lett.* **8**, 48 (1966).